LANGMUIR Article
Cite This: Langmuir 2018, 34, 3604−3609
pubs.acs.org/Langmuir

Opposite Surface and Bulk Solvatochromic Effects in a Molecular Spin-Crossover Compound Revealed by Ambient Pressure X-ray Absorption Spectroscopy

Francesco Borgatti,[†] Piero Torelli,[‡] Marco Brucale,[†] Denis Gentili,[†] Giancarlo Panaccione,[‡] Celia Castan Guerrero,[‡] Bernhard Schäfer,[§,⊥] Mario Ruben,*[,§,⊥] and Massimiliano Cavallini*[,†]

[†]Consiglio Nazionale delle Ricerche, Istituto per lo Studio dei Materiali Nanostrutturati (CNR-ISMN), Via P. Gobetti 101, Bologna 40129, Italy

[‡]CNR-IOM, Tasc Laboratory, S.S. 14 Km 163.5 in Area Science Park, Basovizza, Trieste 34149, Italy

[§]Institute of Nanotechnology, Karlsruhe Institute of Technology, Eggenstein-Leopoldshafen D-76344, Germany

[⊥]Institut de Physique et Chimie des Matériaux de Strasbourg (IPCMS), CNRS-Université de Strasbourg, 23, rue du Loess, BP 43, Strasbourg Cedex 2 67034,France

ABSTRACT: We investigate the solvatochromic effect of a Fe-based spin-crossover (SCO) compound via ambient pressure soft X-ray absorption spectroscopy (AP-XAS) and atomic force microscopy (AFM). AP-XAS provides the direct evidence of the spin configuration for the Fe(II) 3d states of the SCO material upon in situ exposure to specific gas or vapor mixtures; concurrent changes in nanoscale topography and mechanical characteristics are revealed via AFM imaging and AFM-based force spectroscopy, respectively. We find that exposing the SCO material to gaseous helium promotes an effective decrease of the transition temperature of its surface layers, while the exposure to methanol vapor causes opposite surfacial and bulk solvatochromic effects. Surfacial solvatochromism is accompanied by a dramatic reduction of the surface layers stiffness. We propose a rationalization of the observed effects based on interfacial dehydration and solvation phenomena.

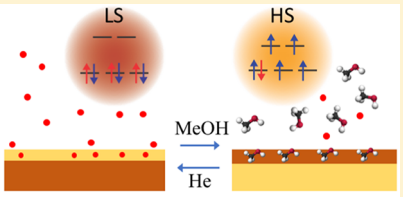

INTRODUCTION

Spin-crossover (SCO) compounds are transition metal complexes exhibiting spin-state switching under certain conditions; the transition is accompanied by changes of a variety physical properties such as color, dielectric constant, conductivity, and mechanical properties.[1−4] Spin-state switching is primarily exhibited by octahedral complexes of 3d transition metal ions having d4 to d7 ground-state configurations; these complexes populate low-spin (LS) or high-spin (HS) electron configurations depending on whether the ligand field is respectively lower or higher than the spin pairing energy. LS/HS transition can be induced by different external stimuli such as temperature, pressure, solvent inclusions, electrical fields, or light.[1−3,5,6] Because of the large variety of physical properties that can be switched together with the spin transition, and the recent improvement in their stability and processability,[7−10] SCO compounds were proposed for a variety of technological applications ranging from electronic/spintronic to chemical/pressure sensors,[3,11−18] in which surfaces and interfaces play a crucial role. In this framework, the application for gas sensor devices in which the temperature of the LS/HS spin transition can be tailored through the inclusion of gas or solvent molecules into the crystalline structure, is particularly important because of its direct technological implications.

The inclusion of solvent molecules into the crystalline structure modifies the splitting of the 3d orbitals of the metal atom, shifting its spin transition temperature. This effect, which is often made evident by a change of color (solvatochromic effect), has been observed for many materials but it is particularly important in SCO complexes[14,19−21] since it changes the spin state and all the physical properties associated with it, thereby enabling SCO compounds as ideal candidates for multiparametric (multimodal) sensing applications.[22] In view of this, a deep study of the spin state of surfacial layers is of crucial importance. Here, we employ ambient pressure soft X-ray absorption spectroscopy (AP-XAS) and atomic force microscopy (AFM)-based nanomechanical characterization to probe the spin state switching of the SCO model compound ($[Fe(L)_2]$ (LH: (2-(pyrazol-1-yl)-6-(1H-tetrazol-5-yl)pyridine) (**1**)[23] (whose chemical structure is shown in the Scheme 1) promoted by exposure to pure gaseous helium or methanol-vapor-saturated helium atmosphere (He+MeOH). Our results demonstrate an active role of He in promoting partial surface dehydration of **1** crystals, and an opposite solvatochromic effect on the spin transition temperature at the crystal surface with respect to the bulk upon exposition to methanol vapors (i.e., a ST temperature reduction in the bulk and a ST temperature increase in the surface layers).

Received: January 4, 2018
Revised: March 6, 2018
Published: March 6, 2018

DOI: 10.1021/acs.langmuir.8b00028
Langmuir 2018, 34, 3604−3609

Scheme 1. Chemical Structure of ([Fe(L)$_2$] LH: (2-(Pyrazol-1-yl)-6-(1H-tetrazol-5-yl)pyridine (1)

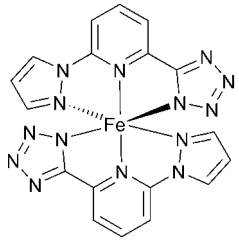

1

EXPERIMENTAL SECTION

Ambient Pressure XAS. The experiment has been performed by AP-XAS on the APE-HE beamline of the Italian synchrotron radiation facility (Elettra). The measurement of the XAS spectra of samples in ambient condition is well established in the hard X-ray regime while still relatively new in the soft X-ray range where however lie some of the most interesting absorption thresholds like the $L_{2,3}$ edge of the transition metals. The recording of the XAS spectra in total electron yield (TEY) which ensure the high surface sensitivity of the measurement, is another qualifying point of the present measurement: once again the XAS spectra in ambient conditions are commonly performed in photon out experiments and rarely with electron detection to avoid problems with the electron mean free path in gases, but at the expense of the surface sensitivity.

The AP-XAS system consists essentially of a reactor cell with a gas fluxing circuit and a Si_3N_4 membrane (window), of 100 nm of thickness which permits the transmission of the incident soft X-ray beam without significant loss of intensity in the photon energy range of interest. Figure 1 shows a schematic cross-section of the reactor cell

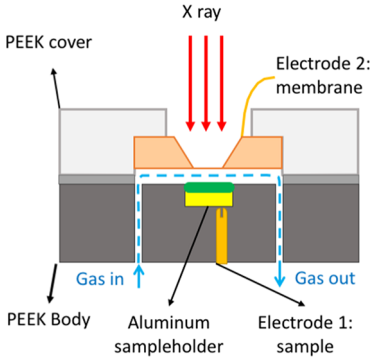

Figure 1. Schematic cross section of the reactor cell used for measurement. The orange layer is the SiN membrane; the green line is the sample while the dotted blue lines represent the gas circuit. The body of the cell (represented in gray) is made of polyether ether ketone (PEEK) an UHV compatible and chemically inert polymer material.

used for measurement. The membrane and the sample are electrically isolated. The window is a Si_3N_4 membrane (500 μm × 500 μm size and 100 nm thickness in square supporting frames of 10 × 10 mm^2 size and 200 μm thickness). The choice of the SiN membrane thickness has been a compromise between high transmission and mechanical strength. The X-ray transmission through the membrane is approximately 70% for photons of 700 eV. The sample is glued onto an aluminum support which is floating from ground and connected with a coaxial cable. In this geometry, the X-ray pass thought the membrane and the gas layer, then hit the sample and generate the secondary emission which is collected by a picoamperometer connected to the sample and measuring the drain current. All the measurements were performed keeping the sample grounded through the picoamperometer and applying a positive bias voltage of 90 V to the membrane.

A saturated He+methanol mixture was obtained by fluxing 100 mL of helium per minute through a chemical bubbler containing absolute methanol (Aldrich 99%).

Atomic Force Microscopy and Nanomechanical Characterization. AFM imaging and force spectroscopy were performed on a Multimode 8 microscope equipped with a Nanoscope V controller and a type JV piezoelectric scanner. Samples were scanned in PeakForce mode with NTMDT-NSG10 probes (Spectrum Instruments, Ireland) in a closed fluid cell under a constant He flow. In some of the experiments, He was saturated with methanol vapor immediately prior to its injection in the fluid cell. Raw images were processed with Gwyddion 2.48 (http://gwyddion.net/). AFM mechanical characterization was performed by recording multiple point-and-shoot force vs distance curves in the same set of locations in presence and absence of methanol. The deflection sensitivity of each probe was determined on a silicon oxide surface, and its spring constant was measured with the thermal noise method.

Nanoscratching experiment were performed by scanning a 250 × 250 nm^2 area in a flat terraced zone of the **1** crystal both in presence and absence of methanol vapors in PeakForce mode by applying a load of 50 nN at each point. He+methanol environment was obtained by fluxing 100 mL of helium per minute through a chemical bubbler containing absolute methanol.

Magnetic Characterization. Details of magnetic characterization was reported in ref.[23]

Optical Microscopy. Optical images were recorded by a Nikon i-80 microscope. The images were recorded by a CCD using 20× and 100× objectives. Details of the setup are reported in refs 24 and 25.

RESULTS AND DISCUSSION

SCO compound **1** shows an LS/HS switching at 295 K, showing a small hysteresis of about 5 K (Figure 2a) and exhibits a very efficient and highly selective solvatochromic effect when exposed to short chain alcohols, as shown in Figure 2b.[22,23,26] In its pristine solid state, **1** forms large red (LS) or yellow/orange (HS) crystals able to include methanol molecules in its

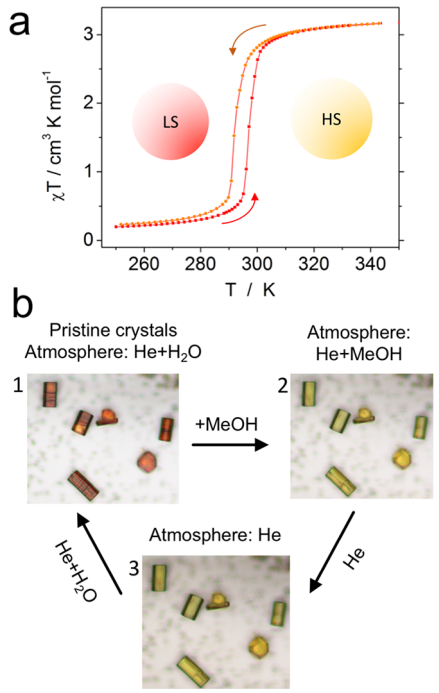

Figure 2. (a) Magnetic characterization of **1**. (b) Optical micrographs of **1** crystallites recorded at room temperature: (b1) Pristine crystallites exposed to He, (b2) during the He+MeOH vapor flux, (b3) exposed to dry He after exposition to He+MeOH.

DOI: 10.1021/acs.langmuir.8b00028
Langmuir 2018, 34, 3604−3609

crystal lattice and disordered water/methanol molecules in cavities present in its structure.[22,23] Upon the exposition to MeOH vapors, the spin transition temperature of **1** decreases to ~248 K.[22] The transition, which affects the whole volume of crystals and is clearly visible by the change of color, occurs in a few seconds and it is fully reversible by removing the MeOH from the environment. The spin transition does not occur by the exposition to pure He; however, once exposed to MeOH, the crystals preserve HS state in dry gas, until their exposition to a moist atmosphere (Figure 2b).

AP-XAS at the Fe $L_{2,3}$ absorption thresholds has been proved to be an excellent element and chemical sensitive approach to monitor in situ changes in the 3d spin configuration promoted at the surface layers of molecular SCO compounds by specific gas or vapor mixtures.[27] The approach is perfectly suited to the Fe(II) ions in **1**; AP-XAS Fe $L_{2,3}$ spectra of **1** kept at 298 K and being sequentially exposed to vacuum and He, are shown in Figure 3. The measurements were performed at the APE-HE

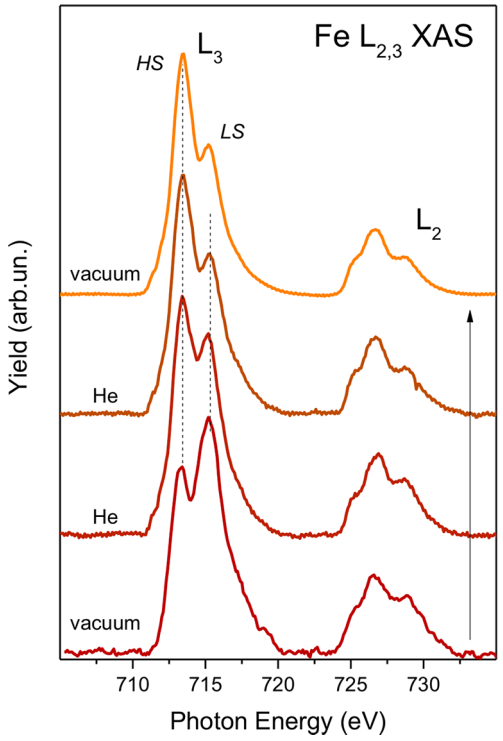

Figure 3. (a) Sequence of Fe $L_{2,3}$ XAS spectra for the SCO powder probed in vacuum or in ambient pressure He environment. The double peak structure for the L_3 absorption edge indicated coexistence of both HS (lower energy) and LS (higher energy) spin state configurations. The background-subtracted spectra are scaled to compare the line shapes. The sequence of the spectra is indicated by the vertical arrow on the right. The color of the spectra is associated with the major LS (brown) or HS (orange-yellow) contribution similarly to what has been observed by optical microscopy.

beamline at Elettra Synchrotron,[28] using a specific setup to acquire XAS spectra while the sample was kept at atmospheric pressure or in low vacuum environment (details in the Experimental Section). Remarkably, the quality of the spectra measured in He atmosphere results very similar to those obtained in vacuum. This is not trivial, considering the different processes involved in the detection of the XAS signal and the application of this technique to a material which contains a rather dilute concentration of Fe ions. All the spectra show a double peak structure for the L_3 absorption edge which for SCO compounds is usually assigned to the coexistence of HS and low LS state configurations.[23,29−31] The energy separation of the two peaks is about 1.7−1.8 eV, in agreement with Fe(II) spectra of similar SCO compounds.[23,29−31] The smearing of the multiplet features expected for these spectra is reasonably explained by the large overlap of the HS and LS spectra, the presence of surface sites blocked in the HS state due to the missing surface bonds,[4] and the room temperature condition for the measurements. Moreover, considering that the probing depth of the signal related to the absorption threshold is of the order of few nanometers, spectral contributions from Fe ions belonging to damaged molecules, or having different chemical states induced by the contamination of the molecular grains during the conservation in air environment before the measurements, cannot be excluded. Despite that, the effect of exposing SCO crystals to pure He is directly evidenced through the variation of intensity of the Fe L_3 peaks, leading to a significant enhancement of the HS spectral contribution. This effect increases progressively with the period of exposure or the number of repeated He/vacuum cycles, thereby indicating large sensitivity of SCO molecules in the surface region to the presence of He atoms. To rule out the dependence of the observed changes from beam damage effects or soft X-ray induced excited spin state trapping effects,[32−34] the measure of extended exposure of the sample to the X-ray beam was probed. The evolution of the spectrum concerns mainly the increase of the LS peak in vacuum with the time (Figure 4). This effect is opposite to the changes observed for the exposure to the He and therefore cannot be the responsible for the observed line-shape changes after He exposure.

The Fe $L_{2,3}$ AP-XAS spectra for a sequence of alternate exposure of **1** powder to He or He+MeOH vapor are shown in Figure 5. The alternated exposure to pure He and He+MeOH

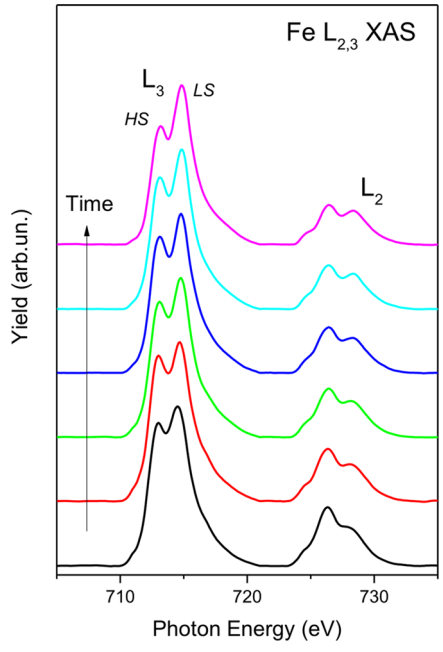

Figure 4. Fe $L_{2,3}$ XAS spectra detected in vacuum to follow the evolution of the spectrum under X-ray irradiation: the intensity of the HS peak is progressively reduced with respect to the LS one. The spectra have been acquired in less than 1 min, waiting for about 10 min of exposure to the X-ray beam among each measurement.

DOI: 10.1021/acs.langmuir.8b00028
Langmuir 2018, 34, 3604−3609

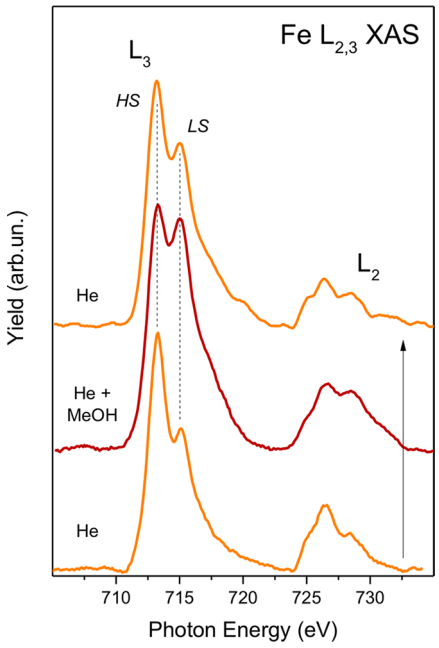

Figure 5. Sequence of Fe $L_{2,3}$ XAS spectra for exposure of the SCO powder to He or He+MeOH ambient pressure atmosphere. The background-subtracted spectra are scaled to compare the line-shapes. The sequence of the spectra is indicated by the vertical arrow on the right. The color of the spectra is associated with the major LS (brown) or HS (orange-yellow) contribution similarly to what has been observed by optical microscopy.

vapor leads to a reversible change of the HS/LS intensity ratio in which the HS term is enhanced for exposure to pure He and depressed when MeOH is present in the chamber, corresponding to an effective shift of the transition temperature toward higher temperatures for the surface region of the SCO sample measured by AP-XAS. Surprisingly, this trend is actually the opposite of the one observed for the bulk of this material by magnetic, spectroscopic and optical measures, the latter clearly showing a predominant HS state upon the exposition to methanol atmosphere.[22]

We explain the effect of dry He atmosphere as a dehydration of the surface layers of the crystals. Because of the porosity of **1** crystals, a fraction of He atoms are adsorbed into the cavities of the crystals inducing partially displacing adsorbed water molecules[35] originally present in the cavities, generating a distortion in the structure that causes the shift of the transition temperature of surface layers below RT. This interpretation fits with the effect observed by heating the **1** crystals to the transition temperature, at which some molecules of methanol are desorbed causing the crystal fragmentation.[22] As the crystals are exposed to a moist atmosphere, water molecules are reintegrated in the pores of surface layers. Due to the fact that the no effects were observed transition by XAS by simple exposition to vacuum, we concluded that He must have a role in this desorption, probably inducing the dehydration. More intriguing is the effect of methanol saturated atmosphere on the spin state of the surface layers. As the observed behavior by AP-XAS exposition to MeOH vapor is limited to surfacial layers, we investigated the effect of MeOH atmosphere on morphology and nanomechanical properties.

AFM-based imaging and force spectroscopy are ideal tools to investigate the morphology and the mechanical behavior of materials at the nanoscale; we employed both of them to corroborate the evidence gathered through AP-XAS with a completely uncorrelated technique. The nanoscale surface morphology of **1** crystals observed by AFM under He flux exhibits a mixture of rough areas comprising multiple crystallites in the same micrometer-squared scale area (observed r.m.s. roughness S_q = 83 ± 54 nm), and large flat terraced areas (S_q = 2.6 ± 0.8 nm, terrace step = 0.9 ± 0.2 nm) with occasional cracks (Figure 6). In some areas, an additional set of higher (step height = 1.7 ± 0.2 nm), parallel linear features crossing the previously mentioned terraces is discernible (Figure 6c). When exposed to He+MeOH vapor, only the thicker features disappear (Figure 6e), whereas the shallower terraces remain substantially unaltered, except for an occasionally observed minor reshaping. Figures 6d, f show

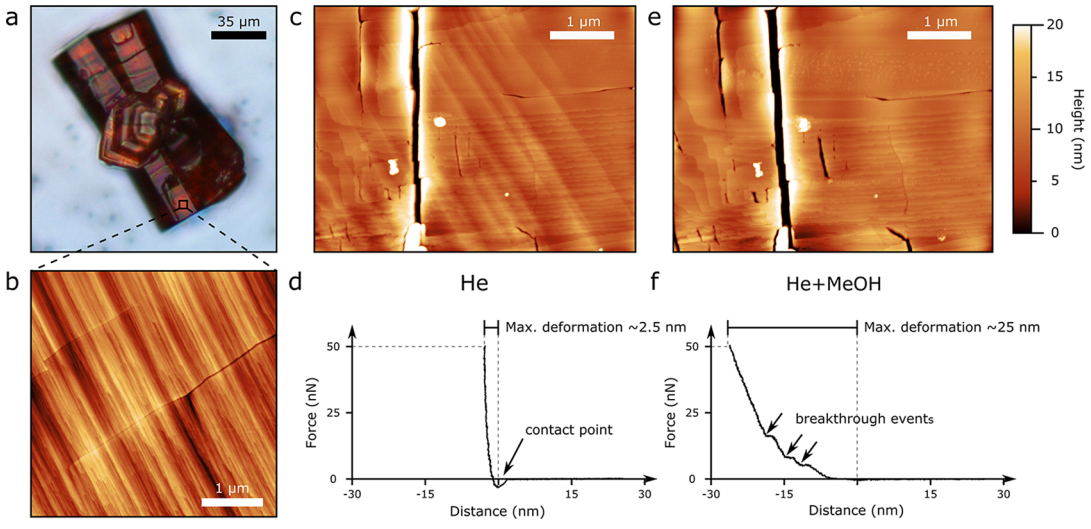

Figure 6. (a) Optical image recorded in air at RT of a **1** crystal. (b) Typical nanoscale morphology of **1** crystals as observed by AFM. (c, e) Persistence and reshaping of different nanoscale terrace features upon exposition to MeOH vapors: (c) recorded in pure He atmosphere, (e) under He+MeOH vapor flux. Only diagonal terrace features evident in panel c disappear in panel e. (d, f) AFM nanomechanical characterization of **1**: representative force/distance traces of the application of a 50 pN load in (d) pure He and (f) in He+MeOH.

DOI: 10.1021/acs.langmuir.8b00028
Langmuir 2018, 34, 3604−3609

typical force/distance curves recorded in He and He+MeOH applying a force of 50 nN. Under He flow, **1** behaves as a comparatively hard material, with a maximum deformation of ~2.5 nm at 50 nN load. Probe/surface interaction is established via a pronounced jump to contact event, probably of electrostatic nature. Conversely, in the presence of methanol vapor, the elastic deformation behavior of the material dramatically changes, reaching a maximum deformation of ~25 nm at 50 nN load. Moreover, in the presence of methanol, nanoindentation breakthrough events are clearly identifiable in most of the recorded curves. During each of these events, the tip penetrates the surface by 1.6 ± 0.1 nm, in accord with the thickness of individual terraces observed via AFM imaging, suggesting that the presence of methanol facilitates the indentation of individual terraces at lower forces. This hypothesis was further substantiated via a nanoscratching experiment performed in presence and absence of MeOH vapors, in which the surface of **1** crystals was found to be prone to plastic deformation only in He+MeOH atmosphere. Nanoscratching experiment were performed by scanning a 250 × 250 nm^2 area in a flat terraced zone of the **1** crystal both in presence and absence of methanol vapors in PeakForce mode by applying a load of 50 nN at each point. Taking an AFM micrograph of the same zone at 1 nN evidenced that the zone scanned at high applied force under methanol flow showed a clear square recessed feature, suggesting the removal of surface material in these conditions. The area scanned at the same force in absence of methanol was instead almost unaffected (Figure 7).

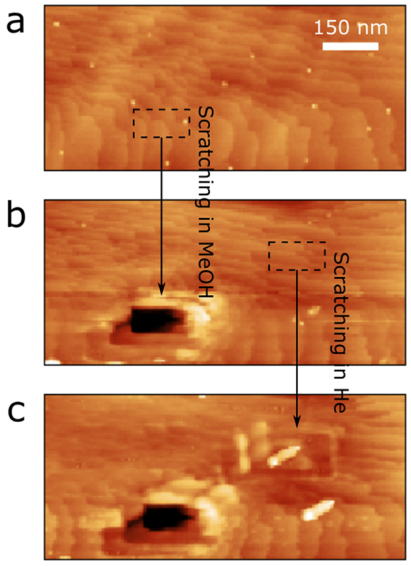

Figure 7. Nanoscratching experiment performed by scanning a 150 × 100 nm^2 area in a flat terraced zone of the **1** crystal (Z scale 0–20 nm). (a) Pristine surface recorded in air. (b) Effect of nanoscratching performed in He+MeOH atmosphere applying a loading nanoscratching force of 50 nN. (c) Unsuccessful tentative of nanoscratching performed in He atmosphere applying a loading force of 50 nN.

Even though methanol is not a good solvent for **1**, the observed dramatic reduction of hardness, the spontaneous reshaping of extended features, and the facile indentation upon the exposition to methanol vapors suggest a partial solvation of **1**, limited to a surfacial layer having a thickness of few nanometers. In these conditions, it is thus reasonable to expect surfacial **1** molecules to yield AP-XAS signals closer to those of molecules in solution rather than in the volume of crystal grains.

CONCLUSIONS

In conclusion, we have presented for the first time an AP-XAS characterization of solvatochromic SCO performed in methanol saturated atmosphere. The Fe $L_{2,3}$ spectra of the Fe(II) ions belonging to the molecular compound **1** indicate a peculiar behavior of the surface layer, for which an inverse shift of the transition temperature with respect to the bulk structure is observed. We have interpreted these results as promoted by methanol/water adsorption or desorption dramatically modifying the behavior of surface layers. Although this study focused on a SCO model compound, it is reasonable to expect an emergence of analogous bulk/interface effects in many other compounds.

AUTHOR INFORMATION

Corresponding Authors

*E-mail: massimiliano.cavallini@cnr.it.
*E-mail: mario.ruben@kit.edu.

ORCID

Mario Ruben: 0000-0002-7718-7016
Massimiliano Cavallini: 0000-0001-9802-0058

Author Contributions

The manuscript was written through contributions of all authors. All authors have given approval to the final version of the manuscript.

Notes

The authors declare no competing financial interest.

ACKNOWLEDGMENTS

This work has been performed in the framework of the nanoscience foundry and fine analysis (NFFA-MIUR Italy Progetti Internazionali) project and National Flaghship project N–CHEM, NANOMAX.

REFERENCES

(1) Front Matter. In *Spin-Crossover Materials*; John Wiley & Sons: New York, 2013; pp i–xviii.
(2) Gutlich, P.; Garcia, Y.; Goodwin, H. A. Spin crossover phenomena in Fe(II) complexes. *Chem. Soc. Rev.* **2000**, *29*, 419–427.
(3) Bousseksou, A.; Molnar, G.; Salmon, L.; Nicolazzi, W. Molecular spin crossover phenomenon: recent achievements and prospects. *Chem. Soc. Rev.* **2011**, *40*, 3313–3335.
(4) Mikolasek, M.; Felix, G.; Peng, H.; Rat, S.; Terki, F.; Chumakov, A. I.; Salmon, L.; Molnar, G.; Nicolazzi, W.; Bousseksou, A. Finite-size effects on the lattice dynamics in spin crossover nanomaterials. I. Nuclear inelastic scattering investigation. *Phys. Rev. B: Condens. Matter Mater. Phys.* **2017**, *96*, 035426.
(5) Gaspar, A. B.; Seredyuk, M. Spin crossover in soft matter. *Coord. Chem. Rev.* **2014**, *268*, 41–58.
(6) Halcrow, M. A. Structure:function relationships in molecular spin-crossover complexes. *Chem. Soc. Rev.* **2011**, *40*, 4119–4142.
(7) Cavallini, M. Status and perspectives in thin films and patterning of spin crossover compounds. *Phys. Chem. Chem. Phys.* **2012**, *14*, 11867–11876.
(8) Daro, N.; Moulet, L.; Penin, N.; Paradis, N.; Létard, J.-F.; Lebraud, E.; Buffière, S.; Chastanet, G.; Guionneau, P. Spray-Drying to Get Spin-Crossover Materials. *Materials* **2017**, *10*, 60.
(9) Cavallini, M.; Bergenti, I.; Milita, S.; Kengne, J. C.; Gentili, D.; Ruani, G.; Salitros, I.; Meded, V.; Ruben, M. Thin Deposits and

DOI: 10.1021/acs.langmuir.8b00028
Langmuir 2018, 34, 3604–3609

Patterning of Room-Temperature-Switchable One-Dimensional Spin-Crossover Compounds. *Langmuir* **2011**, *27*, 4076−4081.
(10) Gentili, D.; Valle, F.; Albonetti, C.; Liscio, F.; Cavallini, M. Self-Organization of Functional Materials in Confinement. *Acc. Chem. Res.* **2014**, *47*, 2692−2699.
(11) Kahn, O.; Martinez, C. J. Spin-transition polymers: From molecular materials toward memory devices. *Science* **1998**, *279*, 44−48.
(12) Prins, F.; Monrabal-Capilla, M.; Osorio, E. A.; Coronado, E.; van der Zant, H. S. J. Room-Temperature Electrical Addressing of a Bistable Spin-Crossover Molecular System. *Adv. Mater.* **2011**, *23*, 1545−1549.
(13) Linares, J.; Codjovi, E.; Garcia, Y. Pressure and Temperature Spin Crossover Sensors with Optical Detection. *Sensors* **2012**, *12*, 4479−4492.
(14) Naik, A. D.; Robeyns, K.; Meunier, C. F.; Leonard, A. F.; Rotaru, A.; Tinant, B.; Filinchuk, Y.; Su, B. L.; Garcia, Y. Selective and Reusable Iron(II)-Based Molecular Sensor for the Vapor-Phase Detection of Alcohols. *Inorg. Chem.* **2014**, *53*, 1263−1265.
(15) Bartual-Murgui, C.; Akou, A.; Thibault, C.; Molnar, G.; Vieu, C.; Salmon, L.; Bousseksou, A. Spin-crossover metal-organic frameworks: promising materials for designing gas sensors. *J. Mater. Chem. C* **2015**, *3*, 1277−1285.
(16) Cavallini, M.; Melucci, M. Organic Materials for Time−Temperature Integrator Devices. *ACS Appl. Mater. Interfaces* **2015**, *7*, 16897−16906.
(17) Lefter, C.; Rat, S.; Costa, J. S.; Manrique-Juárez, M. D.; Quintero, C. M.; Salmon, L.; Séguy, I.; Leichle, T.; Nicu, L.; Demont, P.; Rotaru, A.; Molnár, G.; Bousseksou, A. Current Switching Coupled to Molecular Spin-States in Large-Area Junctions. *Adv. Mater.* **2016**, *28*, 7508−7514.
(18) Koo, Y.-S.; Galán-Mascarós, J. R. Spin Crossover Probes Confer Multistability to Organic Conducting Polymers. *Adv. Mater.* **2014**, *26*, 6785−6789.
(19) Feltham, H. L. C.; Johnson, C.; Elliott, A. B. S.; Gordon, K. C.; Albrecht, M.; Brooker, S. Tail" Tuning of Iron(II) Spin Crossover Temperature by 100 K. *Inorg. Chem.* **2015**, *54*, 2902−2909.
(20) Rat, S.; Ridier, K.; Vendier, L.; Molnar, G.; Salmon, L.; Bousseksou, A. Solvatomorphism and structural-spin crossover property relationship in bis[hydrotris(1,2,4-triazol-1-yl)borate]iron(ii). *CrystEngComm* **2017**, *19*, 3271−3280.
(21) Fumanal, M.; Jiménez-Grávalos, F.; Ribas-Arino, J.; Vela, S. Lattice-Solvent Effects in the Spin-Crossover of an Fe(II)-Based Material. The Key Role of Intermolecular Interactions between Solvent Molecules. *Inorg. Chem.* **2017**, *56*, 4474−4483.
(22) Gentili, D.; Demitri, N.; Schaefer, B.; Liscio, F.; Bergenti, I.; Ruani, G.; Ruben, M.; Cavallini, M. Multi-modal sensing in spin crossover compounds. *J. Mater. Chem. C* **2015**, *3*, 7836−7844.
(23) Schafer, B.; Rajnak, C.; Salitros, I.; Fuhr, O.; Klar, D.; Schmitz-Antoniak, C.; Weschke, E.; Wende, H.; Ruben, M. Room temperature switching of a neutral molecular iron(ii) complex. *Chem. Commun.* **2013**, *49*, 10986−10988.
(24) Albonetti, C.; Martinez, J.; Losilla, N. S.; Greco, P.; Cavallini, M.; Borgatti, F.; Montecchi, M.; Pasquali, L.; Garcia, R.; Biscarini, F. Parallel-local anodic oxidation of silicon surfaces by soft stamps. *Nanotechnology* **2008**, *19*, 435303.
(25) Cavallini, M.; D'Angelo, P.; Criado, V. V.; Gentili, D.; Shehu, A.; Leonardi, F.; Milita, S.; Liscio, F.; Biscarini, F. Ambipolar Multi-Stripe Organic Field-Effect Transistors. *Adv. Mater.* **2011**, *23*, 5091−5097.
(26) Gentili, D.; Liscio, F.; Demitri, N.; Schafer, B.; Borgatti, F.; Torelli, P.; Gobaut, B.; Panaccione, G.; Rossi, G.; Degli Esposti, A.; Gazzano, M.; Milita, S.; Bergenti, I.; Ruani, G.; Salitros, I.; Ruben, M.; Cavallini, M. Surface induces different crystal structures in a room temperature switchable spin crossover compound. *Dalton Trans.* **2016**, *45*, 134−143.
(27) Tamenori, Y. Electron yield soft X-ray photoabsorption spectroscopy under normal ambient-pressure conditions. *J. Synchrotron Radiat.* **2013**, *20*, 419−425.
(28) Panaccione, G.; Vobornik, I.; Fujii, J.; Krizmancic, D.; Annese, E.; Giovanelli, L.; Maccherozzi, F.; Salvador, F.; De Luisa, A.; Benedetti, D.; Gruden, A.; Bertoch, P.; Polack, F.; Cocco, D.; Sostero, G.; Diviacco, B.; Hochstrasser, M.; Maier, U.; Pescia, D.; Back, C. H.; Greber, T.; Osterwalder, J.; Galaktionov, M.; Sancrotti, M.; Rossi, G. Advanced photoelectric effect experiment beamline at Elettra: A surface science laboratory coupled with Synchrotron Radiation. *Rev. Sci. Instrum.* **2009**, *80*, 043105.
(29) Warner, B.; Oberg, J. C.; Gill, T. G.; El Hallak, F.; Hirjibehedin, C. F.; Serri, M.; Heutz, S.; Arrio, M. A.; Sainctavit, P.; Mannini, M.; Poneti, G.; Sessoli, R.; Rosa, P. Temperature- and Light-Induced Spin Crossover Observed by X-ray Spectroscopy on Isolated Fe(II) Complexes on Gold. *J. Phys. Chem. Lett.* **2013**, *4*, 1546−1552.
(30) Lee, J. J.; Sheu, H. S.; Lee, C. R.; Chen, J. M.; Lee, J. F.; Wang, C. C.; Huang, C. H.; Wang, Y. X-ray absorption spectroscopic studies on light-induced excited spin state trapping of an Fe(II) complex. *J. Am. Chem. Soc.* **2000**, *122*, 5742−5747.
(31) Huse, N.; Kim, T. K.; Jamula, L.; McCusker, J. K.; de Groot, F. M. F.; Schoenlein, R. W. Photo-Induced Spin-State Conversion in Solvated Transition Metal Complexes Probed via Time-Resolved Soft X-ray Spectroscopy. *J. Am. Chem. Soc.* **2010**, *132*, 6809−6816.
(32) Collison, D.; Garner, C. D.; McGrath, C. M.; Mosselmans, J. F. W.; Roper, M. D.; Seddon, J. M. W.; Sinn, E.; Young, N. A. Soft X-ray induced excited spin state trapping and soft X-ray photochemistry at the iron L2,3 edge in [Fe(phen)2(NCS)2] and [Fe(phen)$_2$(NCSe)$_2$] (phen[space]=[space]1,10-phenanthroline) [double dagger]. *J. Chem. Soc., Dalton Trans.* **1997**, *0*, 4371−4376.
(33) Davesne, V.; Gruber, M.; Miyamachi, T.; Da Costa, V.; Boukari, S.; Scheurer, F.; Joly, L.; Ohresser, P.; Otero, E.; Choueikani, F.; Gaspar, A. B.; Real, J. A.; Wulfhekel, W.; Bowen, M.; Beaurepaire, E. First glimpse of the soft x-ray induced excited spin-state trapping effect dynamics on spin cross-over molecules. *J. Chem. Phys.* **2013**, *139*, 074708.
(34) Zhang, X.; Costa, P. S.; Hooper, J.; Miller, D. P.; N'Diaye, A. T.; Beniwal, S.; Jiang, X.; Yin, Y.; Rosa, P.; Routaboul, L.; Gonidec, M.; Poggini, L.; Braunstein, P.; Doudin, B.; Xu, X.; Enders, A.; Zurek, E.; Dowben, P. A. Locking and Unlocking the Molecular Spin Crossover Transition. *Adv. Mater.* **2017**, *29*, 1702257.
(35) Donnet, J. B.; Kobel, L.; Sevenster, A. Helium Adsorption on Solid Surfaces. Study of the Adsorbed Layer by the K Method. *Ind. Eng. Chem. Fundam.* **1974**, *13*, 83−86.

DOI: 10.1021/acs.langmuir.8b00028
Langmuir 2018, 34, 3604−3609